VORONOI APPLIED ELEMENT METHOD FOR STRUCTURAL ANALYSIS: THEORY AND APPLICATION FOR LINEAR AND NON-LINEAR MATERIALS

Kawin WORAKANCHANA[1] and Kimiro MEGURO[2]

ABSTRACT: Voronoi Applied Element Method (VAEM) has been developed based on previous Applied Element Method (AEM). Comparing to the original AEM, the advantage of VAEM can be described as the followings: the boundary of VAEM domain can fit to any type of domain easily, pre-existing joint rather than in the horizontal and vertical direction can be modeled, the model does not require numerical Poisson's ratio, element size can be changed and displacement solution is not depended on the element size. The verification of the model from elastic to non-linear range was shown in the paper. The proposed model shows good compatibility to theories and experimental results.

Key Words: Nonlinear analysis, Discrete elements, Fractures, Failures, Computer analysis

INTRODUCTION

Applied Element Method (AEM) is a numerical model for simulating the structural behavior from an elastic range to a total collapse. In AEM, a structure is modeled as an assembly of rigid elements connected together with a zero-length normal and shear spring as shown in Figure 1. The major advantages of AEM are simple modeling and programming, and high accuracy of the results with relatively short CPU time. By using AEM, highly non-linear behavior, i.e. crack initiation, crack propagation, separation of the structural elements, rigid body motion of failed elements and totally collapse behavior of the structure can be followed with high accuracy (Meguro and Tagel-Din, 1998).

After the first developing for reinforced concrete by Hatem[1)], AEM has been used to simulate behavior of many materials such as soil, mortar and steel (Ramancharla, 2001, Mayorca, 2002, Elkholy, 2003). The model achieves high accuracy in simulating behavior of those materials. However, due to the fact that the model contains only square shape element, it has several disadvantages. To eliminate these disadvantages, the new developed AEM based on Voronoi shape has been proposed.

Each element shape is based on the Voronoi tessellation (Okabe et al., 1992). To represent the physical domain with the Voronoi element, first, the element nodes are given in the space within the domain. Then, we associate all locations in physical domain with the closest member(s) of the element nodal set with respect to Euclidean distance. A region generated by a nodal point represents a Voronoi element.

Using the Voronoi Applied Element Method (VAEM), the element nodes can be placed everywhere in the physical domain with no constraint. Therefore, they can be placed to fit any domain shape

[1] Ph.D. fellow
[2] Professor

without reducing the element size as compared to the original AEM. Moreover, element sizes can be varied and concentrated in interesting areas of interest by varying density of element nodes which reduces the number of elements. Also, the location of the element nodes can be placed to create a weak plane representing pre-existing joint in any direction. In this paper, the formulation of the VAEM was introduced. Last, VAEM was verified in the elastic range and the non-linear range for reinforced concrete materials.

APPLIED ELEMENT METHOD (AEM)

Element Formulation

Considering two rigid bodies connected together with pairs of springs representing stresses and deformations of a hatched area, normal and shear spring's stiffness are defined respectively as shown in the following:

$$k_n = \frac{E \times d \times T}{a} \quad \text{and} \quad k_s = \frac{G \times d \times T}{a} \tag{1}$$

Where, d is the distance between springs, T is the thickness of the element and a is the length of representative area, E and G are the Young's and shear modulus of the material.

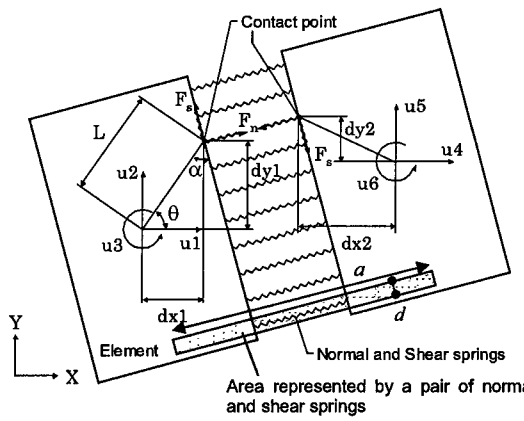

Figure 1. Element shape, Contact Point and Degree of Freedom

Figure 1 shows two AEM elements connected together with a pair of normal and shear springs. Element degrees of freedom are located at the element centroid. The stiffness matrix components corresponding to each degree of freedom are determined by the direct stiffness method. The total element stiffness matrix size is 6x6. Its upper left components are shown in the **Equation 2**.

$$\begin{bmatrix} \sin^2(\theta+\alpha)K_n + \cos^2(\theta+\alpha)K_s & -K_n\sin(\theta+\alpha)\cos(\theta+\alpha) + K_s\sin(\theta+\alpha)\cos(\theta+\alpha) & \cos(\theta+\alpha)K_sL\sin(\alpha) - \sin(\theta+\alpha)K_nL\cos(\alpha) \\ -K_n\sin(\theta+\alpha)\cos(\theta+\alpha) + K_s\sin(\theta+\alpha)\cos(\theta+\alpha) & \sin^2(\theta+\alpha)K_s + \cos^2(\theta+\alpha)K_n & \cos(\theta+\alpha)K_nL\cos(\alpha) + \sin(\theta+\alpha)K_sL\sin(\alpha) \\ \cos(\theta+\alpha)K_sL\sin(\alpha) - \sin(\theta+\alpha)K_nL\cos(\alpha) & \cos(\theta+\alpha)K_nL\cos(\alpha) + \sin(\theta+\alpha)K_sL\sin(\alpha) & L^2\cos^2(\theta+\alpha)K_n + L^2\sin^2(\theta+\alpha)K_s \end{bmatrix} \quad (2)$$

The global stiffness is obtained by standard method for assembling the stiffness of each spring together. Then, the governing equation is

$$[K_G][\Delta]=[F] \quad (3)$$

Failure Criteria

The principal stress concept is used in the original version of AEM. Principal stresses at each spring location are calculated using **Equation 4** as the followings:

$$\sigma_p = \frac{(\sigma_1+\sigma_2)}{2} + \sqrt{\left(\frac{\sigma_1-\sigma_2}{2}\right)^2 + \tau^2} \quad (4)$$

where σ_2 is the secondary stress calculated by

$$\sigma_2 = \frac{x}{a}\sigma_B + \frac{(a-x)}{a}\sigma_C \quad (5)$$

where σ_b and σ_c is normal stress at points (B) and (C) as shown in **Figure 2**, respectively and x is the distant between the calculated location of the principal stress and the perpendicular side. When σ_p exceeds the critical value of tension resistance, the normal and shear springs are considered to be in the failure state. Then, the forces in the normal and shear springs are redistributed in the next increment by applying the normal and shear spring force in the reverse direction.

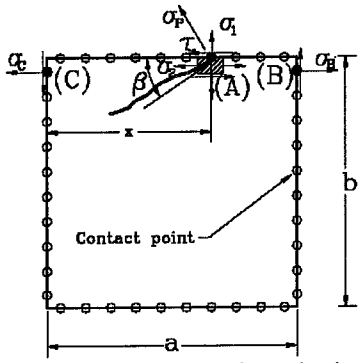

Figure 2. Principal Stress determination

VORONOI APPLIED ELEMENT METHOD (VAEM)

Element Formulation

Again, considering a two-particle subassemblage shown in **Figure 4**, each rigid particle has two

translational and a rotational degree of freedom defined at particle centroid. Assuming small rotations, motion at any points (x,y) of a rigid body can be defined for element 1 and 2 as

$$u_1=u_{c1}-u_3(y-y_{c1}) \quad u_2=u_{c2}+u_3(x-x_{c1})$$
$$u_4=u_{c4}-u_6(y-y_{c2}) \quad u_5=u_{c5}+u_6(x-x_{c2}) \tag{6}$$

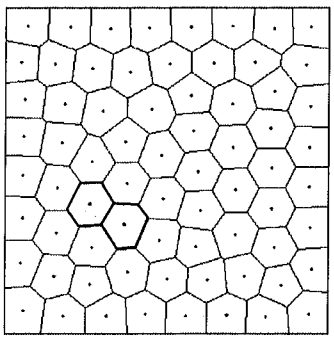

Figure 3. VAEM

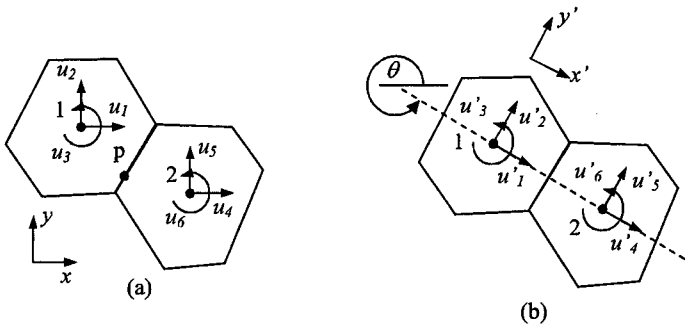

Figure 4. Two-particle assemblage and their degree of freedom (a) global coordinate (b) local coordinate

where u_1, u_2 and u_3 and u_4, u_5 and u_6 are translational displacements and rotation degrees of freedom of element 1 and 2 in global coordinate, respectively. Subscript c specifies the value at the particle centroid. Point p on the boundary surface is separated and defined by p' and p'' after deforming (**Figure 5**). The relative displacement vector of spring deformation in global coordinate at point p can be defined as

$$\overrightarrow{\{\delta_g\}}=p'p''=\begin{Bmatrix}\delta_x\\ \delta_y\end{Bmatrix}=\begin{Bmatrix}u_4-u_1\\ u_5-u_2\end{Bmatrix} \tag{7}$$

Substituting **Equation 6** into **7** and rotating the displacement to the local coordinate paralleled to element surface, we can obtain the relationship between spring deformation in local coordinate and particle displacement in global coordinate as

$$\{\delta_l\}=[\mathbf{R}][\mathbf{B}]\{u\} \tag{8}$$

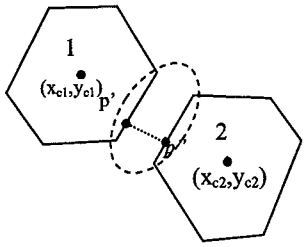

Figure 5. Two-particle assemblage after deformed

where $\{\delta_l\}^T=[\delta_n,\delta_t]$ in which δ_n and δ_t are normal and shear deformation of spring, respectively. Rotational matrix **[R]** = $\begin{bmatrix}\cos\alpha & -\sin\alpha \\ \sin\alpha & \cos\alpha\end{bmatrix}$, deformation-displacement relationship **[B]** = $\begin{bmatrix}-1 & 0 & (y-y_{c1}) & 1 & 0 & -(y-y_{c2}) \\ 0 & -1 & -(x-x_{c1}) & 0 & 1 & (x-x_{c2})\end{bmatrix}$ and $\{u\}^T = [u_1, u_2, u_3, u_4, u_5, u_6]$. Based on the above preliminaries, the strain energy due to spring deformation on the boundary line S can be given as

$$W = \frac{1}{2}\int\{\delta_l\}^T[\mathbf{D}]\{\delta_l\}dS \qquad (9)$$

where the constitutive relationship **[D]**=Diag$[k_{ni},k_{si}]$ in which k_{ni} and k_{si} is stiffness of normal and shear spring number i's, respectively. Applying eq. (8) into (9), we have:

$$W = \frac{1}{2}\{\mathbf{u}\}^T[\mathbf{K}]\{\mathbf{u}\} \qquad (10)$$

where **[K]** = $\sum_{i=1}^{n}\int_{t_i}^{t_{i+1}}[\mathbf{B}]^T[\mathbf{D}][\mathbf{B}]dS$ is the stiffness matrix due to all springs on the boundary. t_i and t_{i+1} indicate the initial and last points of the boundary portion i, respectively (**Figure 6**). By applying Castigliano's theorem to **Equation 5**, stiffness Equation can be derived as

$$\{r\} = \frac{\partial \mathbf{V}}{\partial \mathbf{u}} = [\mathbf{K}]\{\mathbf{u}\} \qquad (11)$$

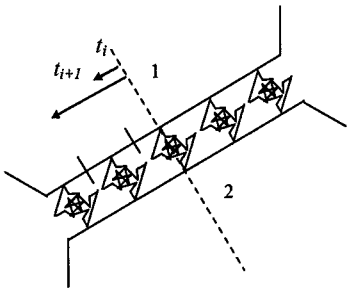

Figure 6. Normal and shear spring at element boundary

where {r} contains the generalized force components associated with each displacement vector {u}.

Equivalent continuum

Relationship between discrete constants k_{ni} and k_{si} and the elastic properties in this study follows the equivalent continuum method (Morikawa et.al., 1985). The method employs the equivalence of strain energy between discrete system and continuum and the advantage of close-pack circular discrete element geometry. To apply with AEM, it was found in the formulation process that these relationships are almost the same as the original proposed but times with square root 3. Therefore, this relationship for AEM is defined as

Plane stress:

$$k_{ni} = \frac{E \cdot t}{(1-\nu) \cdot d}, k_{si} = \frac{E \cdot t \cdot (1-3\nu)}{(1-\nu^2) \cdot d} \tag{12}$$

Plane strain:

$$k_{ni} = \frac{E \cdot t}{(1-2\nu)(1+\nu) \cdot d}, k_{si} = \frac{E \cdot t \cdot (1-4\nu)}{(1-2\nu)(1+\nu) \cdot d} \tag{13}$$

where E is elastic modulus, ν= Poisson's ratio, t = material thickness perpendicular to plane and d = distance between two particles. It should be noted that the Poisson's ratio is limited from -1 to 0.33 for plain stress and -1 to 0.25 for plain strain to prevent a negative value of tangential stiffness.

LOCATION OF ELEMENT NODES AND SPRINGS

In the original square AEM, the element node is placed at the center of the element and the springs are distributed around the center of element side. Due to its square shape, the line connected between two nodes passes through the centroid of distributed spring therefore no eccentric forces occur when loading is applied. In contrary, VAEM does not possess this property. If we put the element node at the center of gravity and distribute the spring around the center of element's side according to the previous version, the sum of the distributed spring force on an element side will not pass through the element node and create an unbalanced moment which affects the rotation at the material point, which is not considered realistic in case of continuum material. The alternative is to put the element node at the Voronoi nuclei and put the center of distributed spring at the middle point between these nodes which is the element boundary according to Voronoi diagram property, thus all of the eccentric forces are eliminated.

STRESS CALCULATION

In VAEM, stresses can be classified into two types; spring's stress and stress at the element node. Spring normal and shear stress can be calculated by dividing spring force in each spring by their areas. Unlike the spring stresses, the stresses at the element node are calculated using all springs around the element. This method was first proposed by Bolander[6]. To calculate stresses at any plane passing through the element node, the internal forces on the plane required for equilibrating the force in the half plane of element (**Figure 7**) are calculated (**Equation 14**). Then, stresses can be calculated by dividing these forces with the area of that plane (**Equation 15**).

$$\begin{aligned} F_{n\theta} &= \sum_{i}^{n} R_i [F_{ni} \cos(\pi - \alpha_i + \theta) + F_{ti} \cos(\alpha_i - \theta)] \\ F_{t\theta} &= \sum_{i}^{n} R_i [F_{ni} \cos(\pi - \alpha_i - \theta) + F_{ti} \cos(\alpha_i + \theta)] \end{aligned} \tag{14}$$

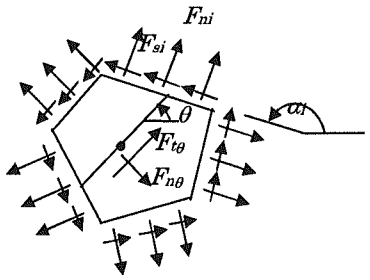

Figure 7. Force calculation at the element node

Then, stress can be calculated by

$$\sigma_\theta = F_{n\theta}/A_\theta$$
$$\tau_\theta = F_{t\theta}/A_\theta \qquad (15)$$

It is noted that we can calculate σ_{xx}, σ_{yy} and τ_{xy} using

$$\sigma_{xx} = F_{n\theta}/A_\theta \quad \text{when} \theta=0^\circ$$
$$\sigma_{yy} = F_{n\theta}/A_\theta \quad \text{when} \theta=90^\circ$$
$$\tau_{xy} = F_{t\theta}/A_\theta \quad \text{when} \theta=0^\circ \qquad (16)$$

VERIFICATION FOR ELASTIC BEHAVIOR

In this section the behavior of VAEM in elastic range was verified by analyzing an elastic square box, cantilever beam, deep beam and circular disk.

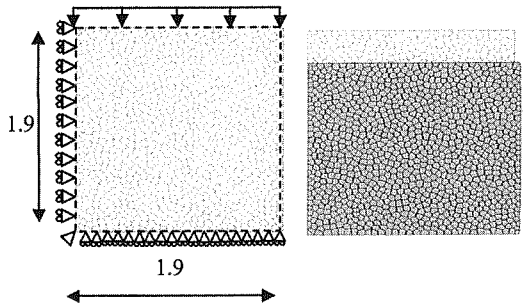

Figure 8. VAEM geometry and loading and VAEM after deformation

Elastic Analysis of Square Box under the Uniform Compressive Force

A box of width 1.9, height 1.9 and thickness 1 units is fixed at the bottom and left side (Figure 8). It is loaded from top by displacement control. Young's modulus was varied from 1000 to 3000 and Poisson's ratio was varied from 0.0 to 0.3.

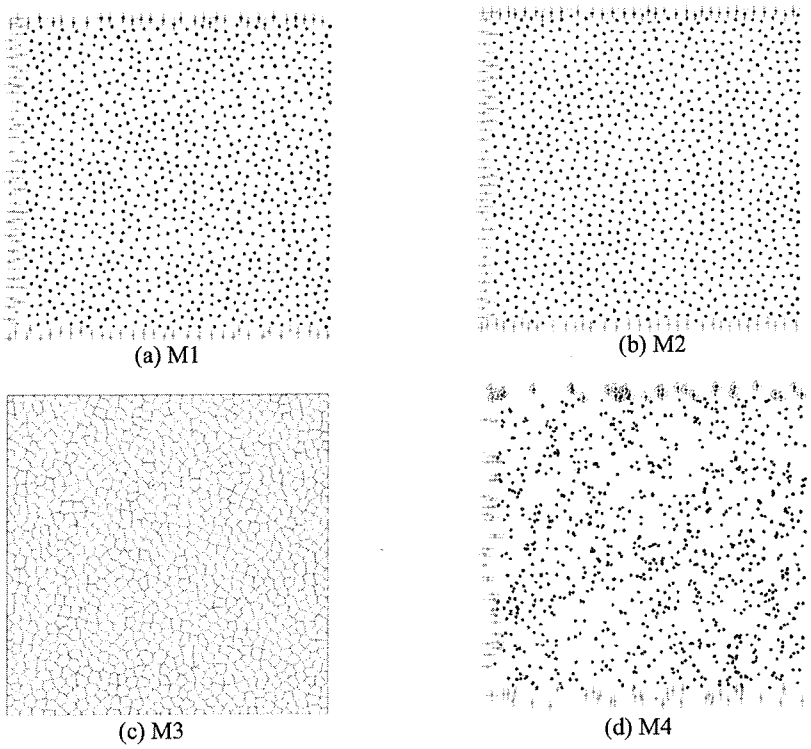

(a) M1 (b) M2

(c) M3 (d) M4

Figure 9. VAEM mesh

General VAEM mesh – Effect of element arrangement

Several VAEM meshes were tested to investigate the parameters affecting the elastic behavior. The first example shows the behavior of square box under the uniform compressive force in plain stress case (**Figure 8**). Mesh M1, M2 and M3 were generated by controlling the distance between each element (**Figures 9(a) to 9(c)**). Mesh 4 is randomly created without any constraint (**Figure 9(d)**). From **Figure 10**, all meshes except for M4 have slightly effect on the elastic Poisson's ratio. The result of varying E in **Figure 11** at $\nu = 0$ shows good agreement between theoretical and numerical value.

Cantilever beam

The cantilever beam with a cross-section of 1x1 m^2 and 10 m span is subjected to a point load at the free end (**Figure 12**). Young's modulus is 2.14×10^7 kN/m^2 and Poisson's ratio is 0. The displacement obtained from VAEM and original AEM are shown in the **Table 1**. It was found that, both square shaped and Voronoi shaped AEM results match well with the theoretical result.

Deep beam

In this section, the elastic problem of deep beam has been solved and compared with the finite element result (**Figure 13**). A deep beam with a dimension of 2x2 units are loaded at the top with the horizontal load of 5×10^6 units. The comparison of top displacements is shown in the **Table 2**. As shown in **Figure 14**, the stress distribution also matches well with one from FEM. The displacement from VAEM was also compared with the original AEM as shown in **Table 2**. It was shown that the

original AEM show less deformation compared to the VAEM but still both methods give good agreement with the theoretical value.

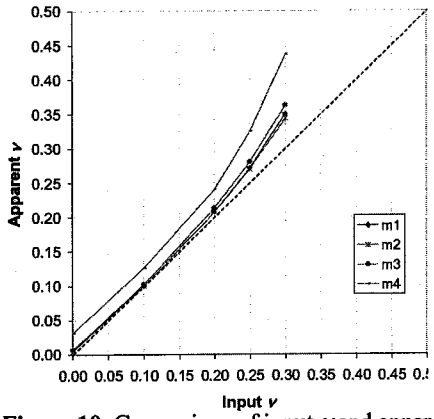

Figure 10. Comparison of input ν and apparent ν

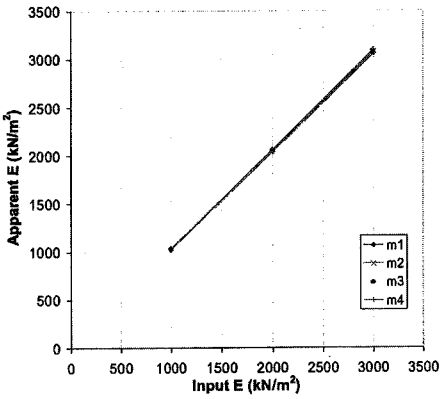

Figure 11. Comparison of input E and apparent E

Table 1. Comparison results of vertical displacement at the cantilever beam tip from VAEM, AEM and exact solution

	Exact ($PL^3/3EI$)	AEM	VAEM
δ_y(m)	9.20	9.12	9.22

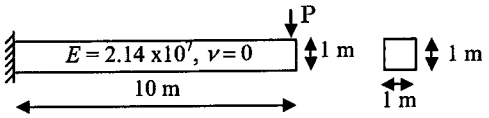

Figure 12. Geometry of cantilever beam

Table 2. Comparison of horizontal displacement in deep beam between VAEM, AEM and FEM

	AEM	VAEM	FEM
δ_x	1.35	1.44	1.46
Difference		1.57%	

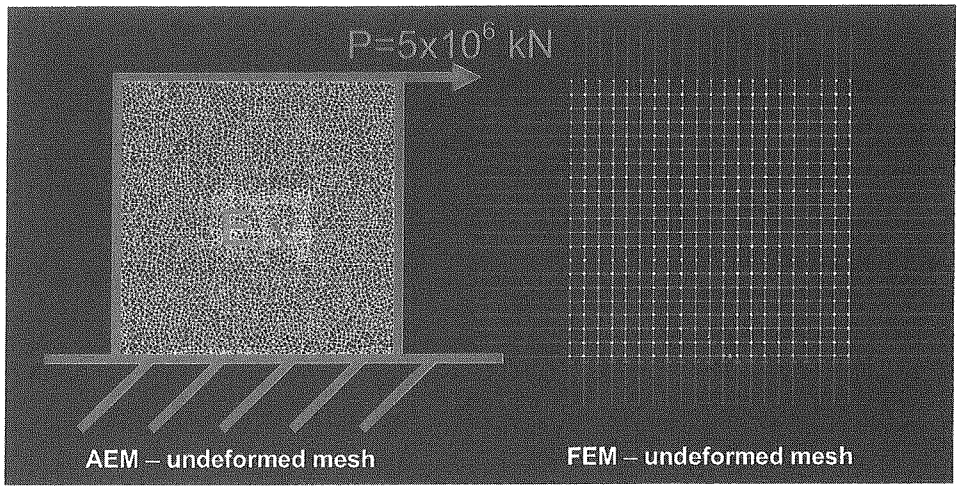

Figure 13. Comparison of σ_{yy} in deep beam

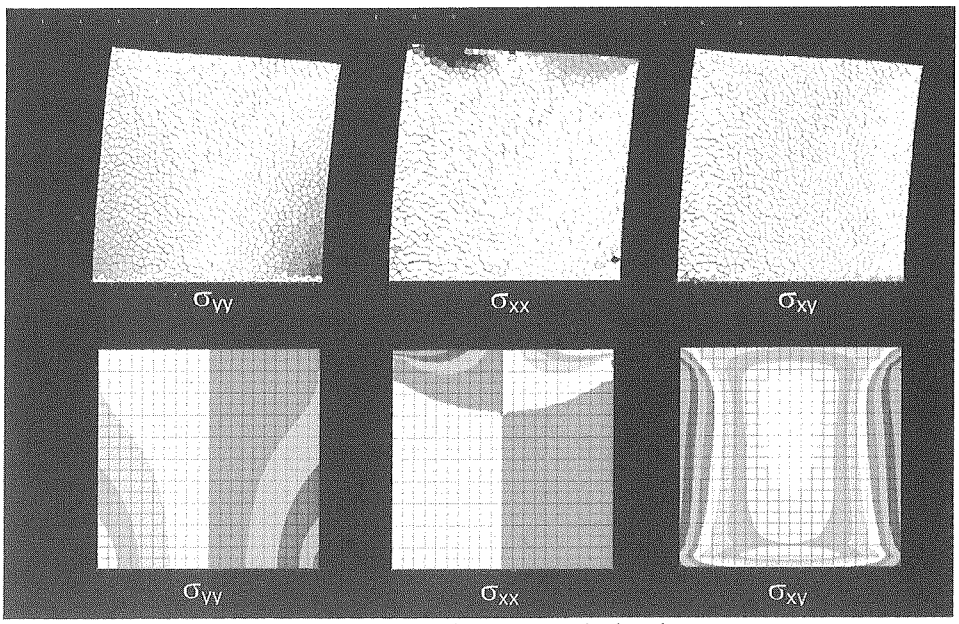

Figure 14. Comparison of stress in deep beam

Circular disk

This example shows the elastic analysis of a circular domain. This type of domain requires a large number of elements in the original AEM to obtain the accurate result due to its single size square-shaped element. **Figure 15** shows the VAEM mesh of circular disk of 8 unit diameter subjected to two point loads from the top and bottom of the disk. In this problem, the Young's modulus is 2.14×10^7 units. The stress distribution at the center line was compared with the theory of elasticity and a good agreement result is observed.

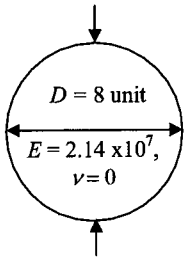

Figure 15. Circular disk with vertical applied load

The plot of σ_{yy} is shown in **Figure 16(a)** to **16(e)** and σ_{xx} is in **Figure 16 (g)**. From **Figure 16 (a), 16(c), 16 (e)** and the plot in **Figure 17**, it can be seen that stress distribution from VAEM are similar regardless of element size. Moreover, σ_{yy} from **Figure 16(e)** and **16(g)** and the plot in **Figure 17** indicates that the elastic behavior of VAEM is the same regardless of direction. The plot in **Figure 17** indicates that stress distribution obtained from VAEM is very close to the exact solution regardless of element size. Stress from the original AEM (solid line with triangular mark) gives a similar result when compare to the exact solution however the difference comes from that fact that there is a difference between the actual and AEM physical domain sizes.

VAEM FOR FRACTURE ANALYSIS OF CONCRETE MATERIAL

The verification of VAEM in simulating plain and reinforced concrete was conducted. The original AEM has capability of tracking the crack distribution without prior knowing the location of the crack. However, the crack distribution is limited to only in the vertical and horizontal direction according to the element shape. With the VAEM, cracks have more freedom to propagate therefore the crack propagation can better follow the real crack path.

CONCRETE MODELING

In this model, the behavior of the material is initially elastic, i.e., $\sigma=E\varepsilon$, where E is the apparent concrete Young's modulus. Inelastic behavior is formulated based on similar concept of stress-strain boundary introduced by Cusatis et al. (2003). Elastic behavior is limited by three boundaries, which are tension-shear, compression-shear and compression as shown in **Figure 18**. This concept is based on the normal and shear stress in the springs rather than the tensorial measure of stress which can be biased based on the mesh configuration. Schlangen (1995) used a criteria based on stress measures computed at the nodes of a beam lattice, rather than in the beams themselves. Moreover, Meguro and Hatem (1998) employed the principal stresses concept similar to the use of tensorial measure by Schlangen however principal stresses is calculated at the springs themselves instead of element nodes. Employing one of the two methods is expected to reduce the mesh bias on the fracture criteria. The study will be conducted in the near future. If the force reaches tension-shear boundary, the crack is occurred and the stiffness of the spring is assumed as 0.01 of the initial stiffness and all of the forces in normal and shear springs are redistributed. If the force reaches the compression shear and compression boundary, the stiffness of the spring is also assumed as 0.01 of the initial stiffness however no force is redistributed.

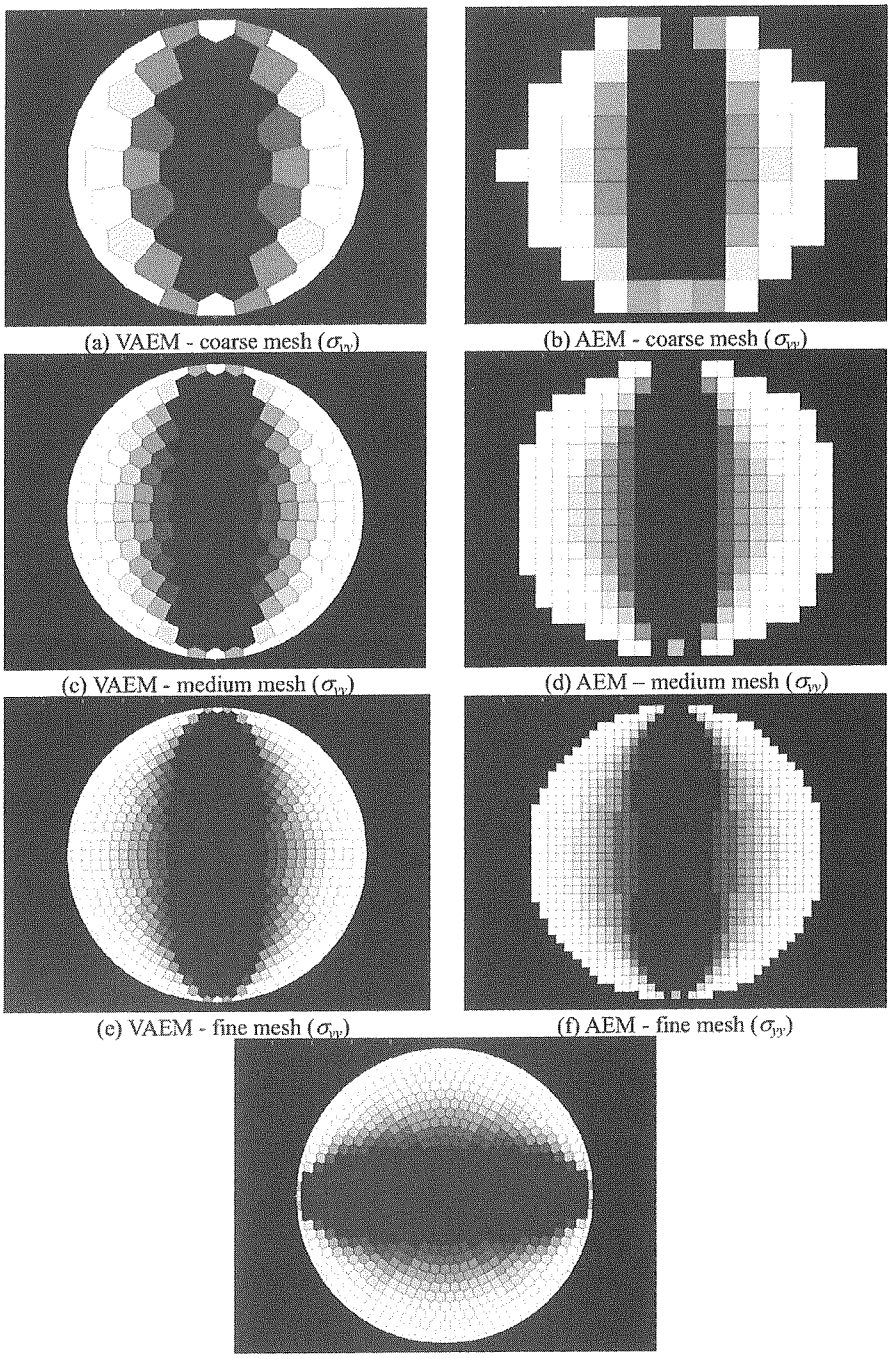

Figure 16. Comparison of stress distribution form VAEM and AEM

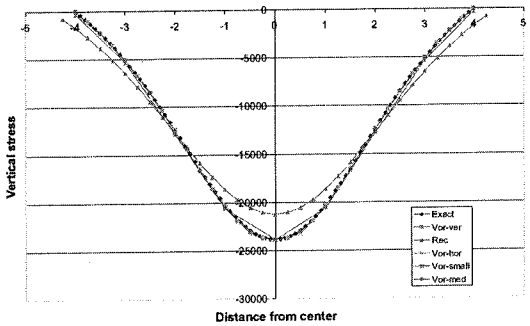

Figure 17. Stress comparison of AEM, VAEM and exact solution

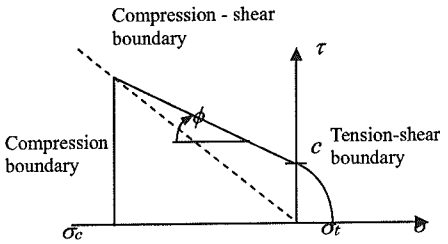

Figure 18. DEN test set up

PURE CONCRETE MODELING

In this section, the fracture behavior of plain concrete structure was simulated using VAEM. The crack propagation was compared with the experimental result.

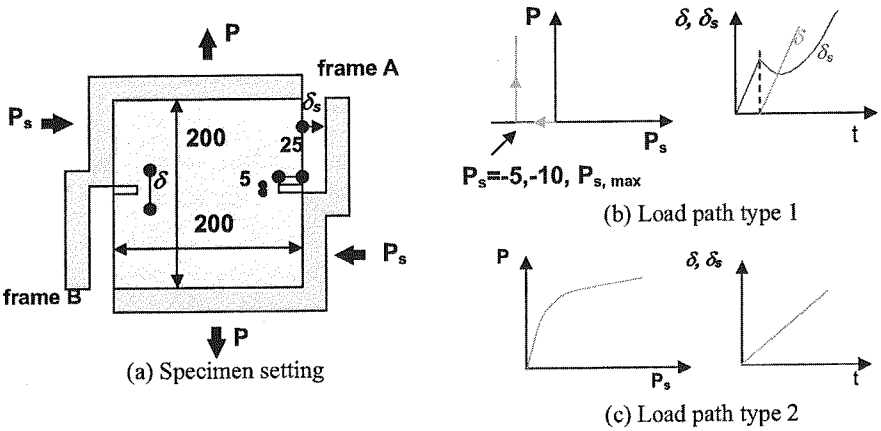

Figure 19. DEN test set up

Double-Edge-Notch Specimen (DEN)

VAEM and original AEM were used to simulate the test of DEN specimens by Nooru-Mohamed et al. (1993). Six specimens with dimension of 200x200 mm were subjected to 2 types of load-paths

(**Figure 19(a)**). The first is axial tension at a constant shear force. In this case, a compressive shear load P_s was applied to the specimen in displacement control until P_s = -5 kN, -10 kN and to the maximum shear load that the specimen could sustain. Then the axial tension P was applied (**Figure 19(b)**). The second load-path is called 'proportional loading' (**Figure 19(c)**), i.e., an axial tensile and a lateral compressive shear load were applied to the specimen such that the ratio of axial deforamtion (δ) to lateral deformation (δ_s) remained constant throughout the test. **Figures 21 and 22** show the comparison between simulation and test results. From the observation, the crack propagation between experimental and simulation in each case are in good agreement.

REINFORCED CONCRETE MODELING

In this section, VAEM was used to simulate the reinforced concrete behavior in the monotonic static loading condition. The numerical results are compared with the experiment results in the following sections.

Reinforcement model

The reinforcement was modeled by adding in normal and shear springs as shown in **Figure 20**. In this study, perfectly plastic model was used for reforcing bars to represent yielding as also shown in **Figure 20**.

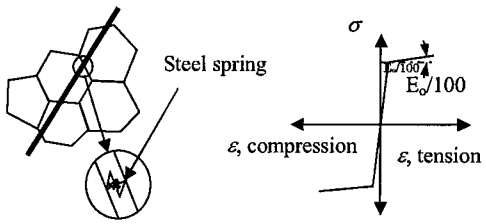

Figure 20. Steel springs and their material properties

Size effect analysis

A simulation of two beams out of totally six beams from experiment was performed. The original test was carried out by Iguro et al. (1985). These beams were not provided with shear reinforcement. The material properties for beam b-1 and b-5 were shown in **Table 3**. Beam b-1 and b-5 are selected for the simulation. The beam dimensions, reinforcement as well as load-deformation behavior are shown in **Figures 23 and 24**. A loading is uniformly applied with water pressure system. The main reinforcement ratio "pr" in the vicinity of the supporting, where shear failure would occur, was 0.4% and it was 0.8% in the middle of the beam for (b-1) but only 0.4% for the (b-5) case.

Table 3. Material properties of the beams

	Concrete				Steel	
Specimen number	σ_{cu} (MPa)	σ_t (MPa)	pr1	pr2	Diameter (mm)	Yield stress (MPa)
(b-1)	20.2	1.8	0.4%	0.8%	D3	313.8
					D6	431.3
(b-5)	27.9	2.7	0.4%	0.8%	D16	362.8

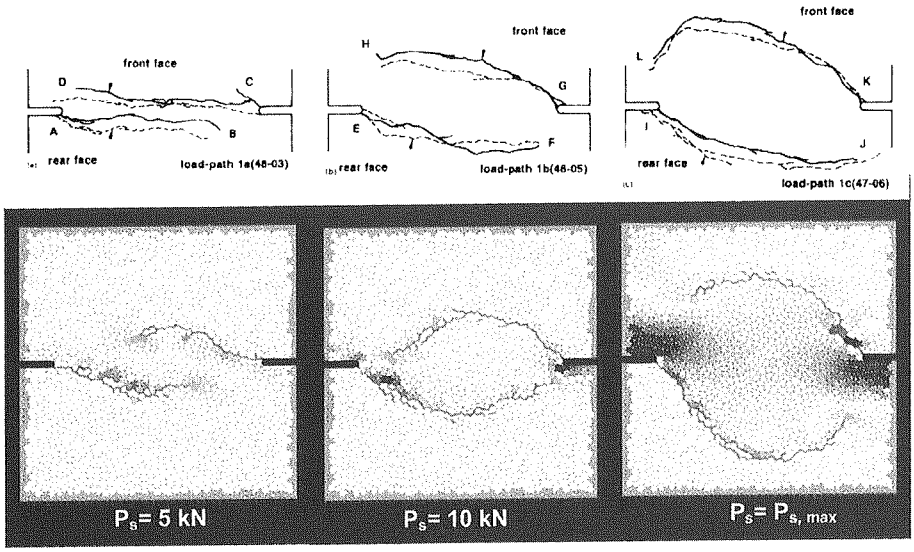

Figure 21. Crack pattern from 1st loading (Color shows σ_{xx})

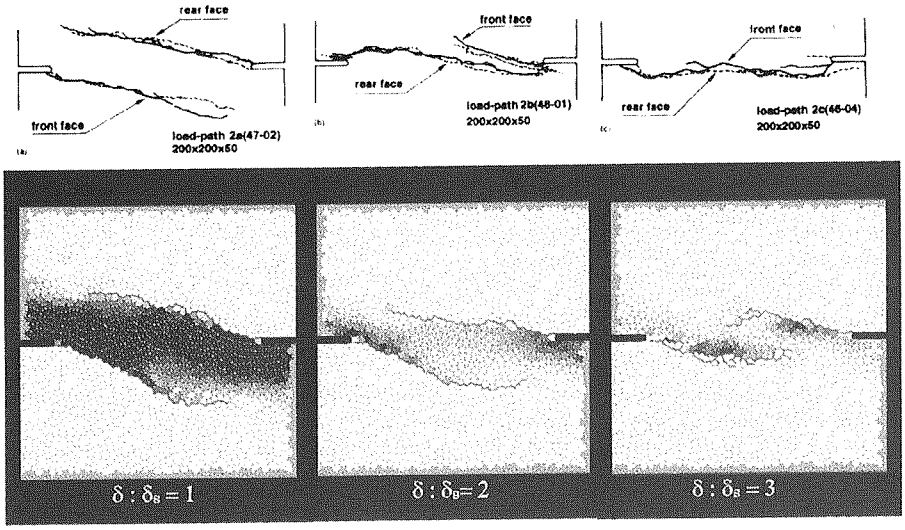

Figure 22. Crack pattern from 2nd loading (Color shows σ_{xx})

Meshes of 1229 and 1449 elements were used in the model for beams (b-1) and (b-2), respectively. Loading was applied using load control condition. The comparison of the force-displacement relationship for beam (b-1) and (b-2) was shown in **Figures 23 and 24**, respectively. It can be seen that the force-deformation relationship obtained from VAEM is close to the experimental results and numerical results from AEM and FEM. However, VAEM exhibits less maximum strength compared to AEM because the diagonal crack in VAEM was represented by a shorter crack length (less zigzag)

which consumes less energy for generating. From **Figures 25** to **27**, it was observed that the crack pattern from VAEM was closer to the actual crack pattern than AEM.

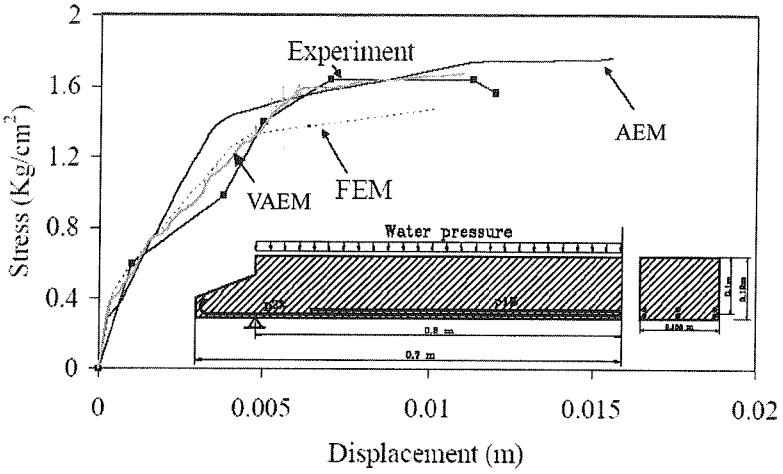

Figure 23. Comparison of stress-displacement relation for beam (b-1)

LARGE DEFORMATION ANALYSIS

To simulate the structural behavior under large deformation, the geometrical change has to be considered during each step of the calculation. This requires the following additional procedures:

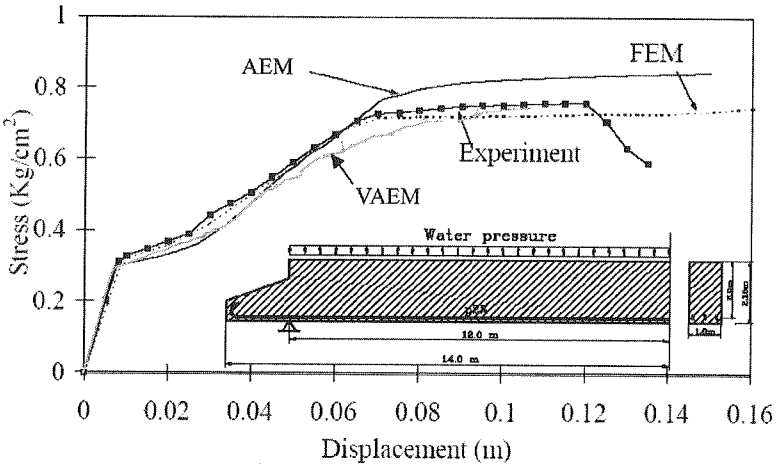

Figure 24. Comparison of stress-displacement relation for beam (b-5)

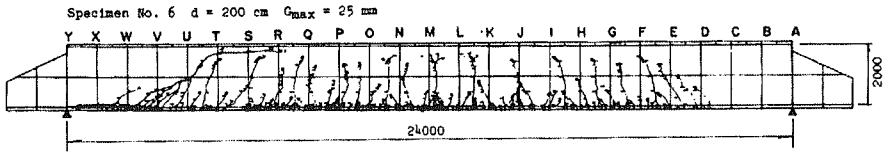

Figure 25. Crack pattern of beam (b-5) from experiment

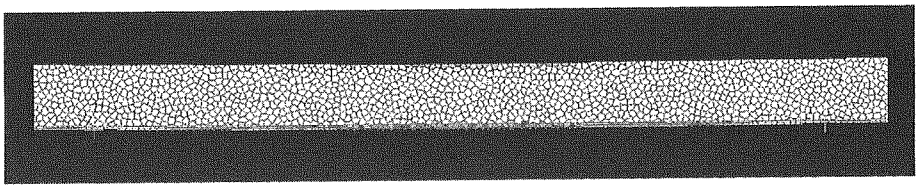

Figure 26. Crack pattern of beam (b-5) from VAEM

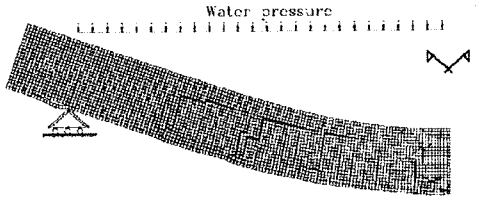

Figure 27. Crack pattern by original AEM

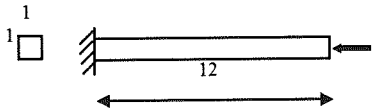

Figure 28. Beam geometry

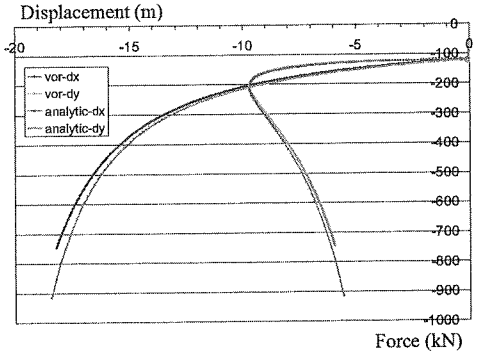

Figure 29. Comparison of the large deformation analysis from numerical model and analytic solution

1) Update the location of the element node according to previously calculated incremental displacement
2) Calculate the geometrical residuals as

$$\{R_G\}=\{f\}-\{F_m\} \tag{17}$$

This is to account for the incompatibility between the external applied forces vector, $\{f\}$ and internal forces, $\{F_m\}$ due to modification of geometry of the structure.
3) Take into account the geometrical residual in the stiffness Equation which can be written as:

$$[K]\{u\} = \{r\}+\{R_G\} \tag{18}$$

The verification of this method was shown in the following paragraphs. The geometry of the beam subjected to a compressive load was shown in **Figure 29**. Young modulus of the beam is equal to $8.4x10^4$. The result obtained from the numerical model was compared with the analytical solution (Timoshenko, S.P. and Gere, J.M., 1961). The results from numerical model predict very closely the theoretical buckling load and force-displacement relationship of the post buckling behavior.

CONCLUSIONS

The VAEM has been developed based on the original AEM. Elastic behavior of VAEM was verified in this section. Comparing to the original AEM, the advantages of VAEM can be described as the followings:

- The model boundary can easier fit any type of domain.
- Pre-existing joint rather than in the horizontal and vertical direction can be modeled.
- The model does not require numerical Poisson's ratio (however Poisson's ratio is limited from -1 to 0.33 in plain stress and -1 to 0.25 in plain strain).
- It is possible to vary element size
- Displacement solution does not depend on the element size

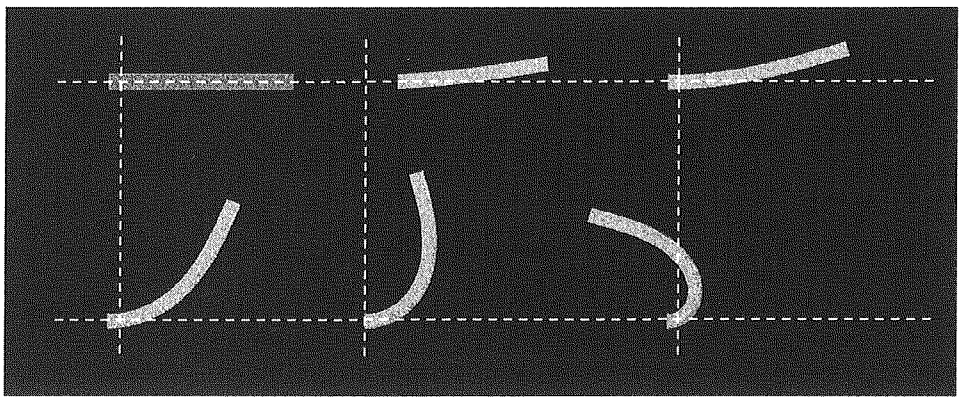

Figure 30. Beam under large deformation

The VAEM was verified for predicting the behavior of plain and reinforced concrete. In all cases, the obtained crack locations agreed well with the experimental results. In case of RC simulation, the crack patterns obtained from VAEM were found to be more accurate than original AEM. Because VAEM

can develop the diagonal better than AEM, VAEM exhibits less maximum resistant compared to AEM.

ACKNOWLEDGEMENT

The first author would like to express his profound gratitude to Japan Ministry of Education, Science and Culture for providing scholarship to pursue this research in Japan.

REFERENCES

Bolander. J., Yoshitake. K., and Thomure J. (1999). "Stress analysis using elastically homogeneous rigid-body-spring networks." *Strucutal Eng./Earthquake Eng.*, 16(2), 125s-162s.

Cusatis, G., Bazant Z. P., and Cedolin, L. (2003). "Confinement-Shear Lattice Model for Concrete Damage in Tension and Compression: I. Theory." *J. Eng. Mech.*, 129(12), 1439-1447.

Elkholy, S. (2003). *Improved Applied Element Method for Numerical Simulations of structural failure and collapse*, Ph.D. thesis, Civil Eng. Dept., The University of Tokyo.

Iguro, M., Shioya, T., Nojiri, Y., and Akiyama, H. (1985). "Experimental Studies on Shear Strength of Large Reinforced Concrete Beam under Distributed Load." *Concrete Library of JSCE*, 5, 137-154.

Mayorca, P. (2002). *Strengthening of unreinforced masonry structures in earthquake prone regions*, Ph.D. thesis, Civil Eng. Dept., The University of Tokyo.

Meguro, K., and Tagel-Din, H. (1998). "Applied element simulation of structures under cyclic loading." *J. Struct. Eng.*, 127(11), 1295-1305.

Morikawa, H., Sawamota Y, and Kobayashi N. (1985) "Local Fracture Analysis of a Reinforced Concrete Slab by Discrete Element Method." *Proceeding of the 1st Conference on Numerical Methods and Fracture Mechanics*, Swansea.

Nooru-Mohamed, M.B., Schlangen, E., and Van Mier, J.G.M. (1993). "Experimental and Numerical Study on the Behavior of Concrete Subjected to Biaxial Tension and Shear." *Advn Cem Bas Mat*, Elsevier, 1, 22-37.

Okabe, A., Boots, B., Sugihara K., and Nok Chiu, S. (1992). *Spatial Tesselation Concepts and Applications of Voronoi Diagrams*, 2nd ed., John Wiley & Sons, New York.

Ramancharla, P. K. (2001). *Numerical analysis of the effects on the ground surface due to seismic base fault movement*, Ph.D. thesis, Civil Eng. Dept., The University of Tokyo.

Schlangen, E. (1995) "Computational aspects of fracture simulations with lattice models." *Fracture Mechanics of Concrete structures*, Wittmann FH, Aedificatio, Freiburg, Germany, 913.

Timoshenko, S.P. and Gere, J.M. (1961). *Theory of elastic stability*, 2nd Ed., McGraw-Hill, New York.